

# Probabilistic inference under time pressure leads to a cortical-to-subcortical shift in decision evidence integration



Hanna Oh-Descher<sup>a,d,\*</sup>, Jeffrey M. Beck<sup>b,d</sup>, Silvia Ferrari<sup>e</sup>, Marc A. Sommer<sup>c,d</sup>, Tobias Egner<sup>a,d,\*\*</sup>

<sup>a</sup> Department of Psychology and Neuroscience, Duke University, Durham, NC, USA

<sup>b</sup> Department of Neurobiology, Duke University, Durham, NC, USA

<sup>c</sup> Department of Biomedical Engineering, Duke University, Durham, NC, USA

<sup>d</sup> Center for Cognitive Neuroscience, Duke University, Durham, NC, USA

<sup>e</sup> Department of Mechanical and Aerospace Engineering, Cornell University, Ithaca, NY, USA

## ARTICLE INFO

### Keywords:

Decision-making  
Satisficing  
Bounded rationality  
Time pressure  
Multi-cue integration  
fMRI

## ABSTRACT

Real-life decision-making often involves combining multiple probabilistic sources of information under finite time and cognitive resources. To mitigate these pressures, people “satisfice”, foregoing a full evaluation of all available evidence to focus on a subset of cues that allow for fast and “good-enough” decisions. Although this form of decision-making likely mediates many of our everyday choices, very little is known about the way in which the neural encoding of cue information changes when we satisfice under time pressure. Here, we combined human functional magnetic resonance imaging (fMRI) with a probabilistic classification task to characterize neural substrates of multi-cue decision-making under low (1500 ms) and high (500 ms) time pressure. Using variational Bayesian inference, we analyzed participants’ choices to track and quantify cue usage under each experimental condition, which was then applied to model the fMRI data. Under low time pressure, participants performed near-optimally, appropriately integrating all available cues to guide choices. Both cortical (prefrontal and parietal cortex) and subcortical (hippocampal and striatal) regions encoded individual cue weights, and activity linearly tracked trial-by-trial variations in the amount of evidence and decision uncertainty. Under increased time pressure, participants adaptively shifted to using a satisficing strategy by discounting the least informative cue in their decision process. This strategic change in decision-making was associated with an increased involvement of the dopaminergic midbrain, striatum, thalamus, and cerebellum in representing and integrating cue values. We conclude that satisficing the probabilistic inference process under time pressure leads to a cortical-to-subcortical shift in the neural drivers of decisions.

## 1. Introduction

Decision-making often involves combining multiple pieces of information, each associated with some degree of uncertainty in predicting an outcome, within a tight deadline. For instance, to determine the best treatment for a patient, a physician would ideally perform an exhaustive set of diagnostic tests and integrate the test results, weighted by their respective reliability. However, this decision process, in addition to being computationally expensive, may take longer than is practical. If the case is urgent, a doctor might forego considering all available tests and base a quick but “good-enough” decision on a subset of information (Lamberts, 2000; Payne et al., 1988; Rieskamp and Hoffrage, 2008; Wright, 1974), a

form of heuristic decision-making known as *satisficing* (Simon, 1956, 1955). While satisficing under uncertainty and high time pressure is ubiquitous in daily life, very little is known about its underlying computational principles and neural mechanisms.

In order to characterize such satisficing strategies, we recently developed a novel, multi-cue probabilistic classification task that allowed us to track the manner in which subjects weight and combine different cues to arrive at their decisions (Oh et al., 2016). Under low time pressure, information was integrated near-optimally across all available cues. By contrast, under high pressure, participants dropped the weaker, less predictive cues from the decision-making process, a satisficing strategy we called “drop-the-worst”. To elucidate the neural dynamics underlying

\* Corresponding author. Department of Psychology and Neuroscience, Duke University, Levine Science Research Center, Box 90999, Durham, NC 27708, USA.

\*\* Corresponding author. Department of Psychology and Neuroscience, Duke University, Levine Science Research Center, Box 90999, Durham, NC 27708, USA.

E-mail addresses: [hanna.oh.descher@duke.edu](mailto:hanna.oh.descher@duke.edu) (H. Oh-Descher), [tobias.egner@duke.edu](mailto:tobias.egner@duke.edu) (T. Egner).

this shift in decision modes from optimal to satisficing, in the present study we combined this task, performed under low (1500 ms) and high (500 ms) time pressure, with functional magnetic resonance imaging (fMRI). Using variational Bayesian inference, we quantified participants' cue usage and related it to changes in regional blood-oxygen-level dependent (BOLD) signals.

While we are not aware of any previous study assessing the neural mediators of probabilistic inference under time pressure, prior reports on statistical learning under stress, and studies of the speed-accuracy tradeoff in perceptual decision-making, offer grounds for tentative hypotheses. Probabilistic inference has been studied extensively through variants of the weather prediction task (Gluck and Bower, 1988; Knowlton et al., 1994), where acquiring probabilistic cue-outcome relationship through feedback has been shown to be associated with activity in the striatum, hippocampus (Knowlton et al., 1996; Poldrack et al., 2001; Shohamy et al., 2004) and parietal cortex (Yang and Shadlen, 2007). In addition, other recent studies of probabilistic decision-making suggest an important role for the frontoparietal attentional control network in mediating learning in a multidimensional decision environment (Niv et al., 2015), and the orbital/ventromedial prefrontal cortex (vmPFC) in encoding expected reward, subjective value, outcome predictions, and credit assignment (Akaishi et al., 2016; Daw et al., 2006; Levy and Glimcher, 2012; O'Doherty et al., 2001).

Stress has been shown to bias decision-making strategies by reducing contributions of the prefrontal cortex (PFC) and encouraging habitual stimulus-response processes (Dias-Ferreira et al., 2009; Schwabe and Wolf, 2009). Specifically, learning the weather prediction task under stress induced by the cold pressor test has been associated with increased use of implicit, striatum-mediated strategies (Schwabe and Wolf, 2012). Similarly, time pressure on perceptual decision-making has been

associated with a deterioration in information processing in early sensory areas (Ho et al., 2012) and increased activity in the striatum (Bogacz et al., 2010; Forstmann et al., 2008), indicating that the striatum may promote faster but possibly premature or sub-optimal decisions.

Here, we characterized how the brain encodes probabilistic cue information as participants shift from employing optimal to satisficing decision strategies with increasing time pressure. Based on the above studies, we predicted that probabilistic decisions will be mediated by both subcortical (striatum, hippocampus) as well as prefrontal (lateral and medial PFC) and parietal regions under low time pressure, with a preferential involvement of the striatum under high time pressure. The data supported this hypothesis and revealed details of the networks involved in this cortical-to-subcortical shift of activity.

## 2. Materials and methods

### 2.1. Participants

Thirty-two healthy volunteers participated in this experiment. Seven participants were excluded from further analysis: Five participants due to chance-level performance and two participants due to excessive head movement ( $> 20$  mm). The final sample consisted of twenty-five subjects (13 females, mean age = 27 years, range = 18–40 years). All participants provided informed consent in line with Duke Medical Center institutional guidelines and were compensated with \$40 for their time (2 h).

### 2.2. Stimuli

The task employed 16 unique compound stimuli (Fig. 1B), constructed by combining four different visual features, color (blue/red),

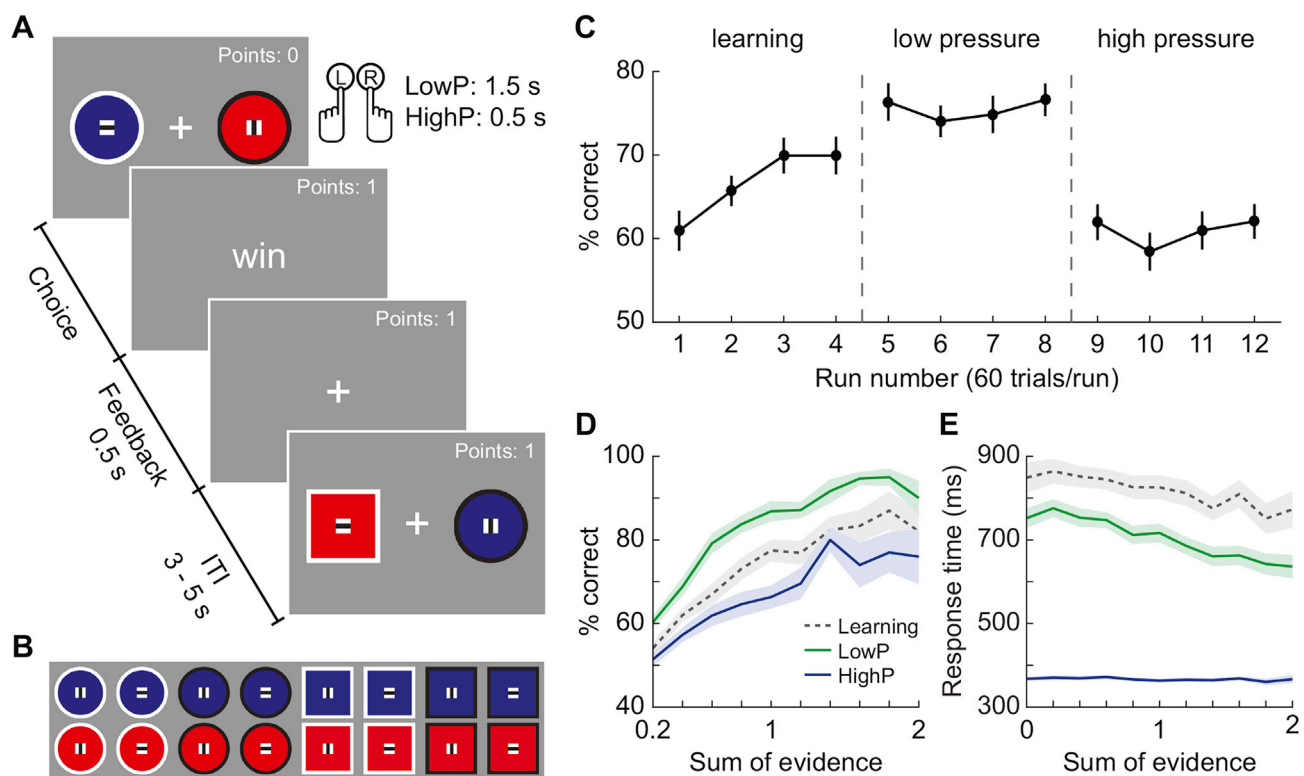


**Fig. 1.** Task design and behavioral results. **A**, Schematic of the multi-cue probabilistic task. Participants were presented with two different compound stimuli, each having four different features or cue dimensions (color, shape, contour, and line orientation). Participants then selected a stimulus that is more likely to win and received a probabilistic outcome (“win” or “lose”). **B**, Sixteen compound stimuli used in the experiment. Each stimulus was paired with all the other stimuli, yielding a set of 120 unique trials. **C**, Behavioral performance throughout the task runs. Plotted is the percentage of correct choices favored by the sum of cue weights, regardless of outcome feedback. Participants completed the low pressure (LowP) and high pressure (HighP) phases inside the fMRI scanner. Error bars indicate SEM. **D**, Percentage of correct choices as a function of objective sum of evidence (SoE). Decision performance significantly improved with increasing SoE in all three experimental phases. **E**, RT as a function of SoE. RT showed significant SoE modulation during the learning and low time pressure phases but this effect disappeared under high time pressure. Shaded area represents SEM.

shape (circle/square), contour (white/black), and line orientation (vertical/horizontal), which we refer to as *cue dimensions*. Each cue dimension was comprised of binary sub-features or *cue states*, each of which was associated with a fixed weight for predicting the probability of winning. These values were complementary and summed to one within each cue dimension. The weights outlined in Table 1 were randomly assigned to the different cue dimensions for each participant at the beginning of the experiment, and every possible weight permutation (24 total) was used at least once. Thus, our neuroimaging analyses focused on encoding of “cue feature-invariant” informational value, by dissociating cue weights from specific cue dimensions and visual features across the subject population.

### 2.3. Multi-cue probabilistic classification task

Participants performed a probabilistic classification task, in which they were asked to compare two compound stimuli and make a prediction about which stimulus is more likely to win (Fig. 1A). The stimuli were sampled from the full set of the 16 compound cues (Fig. 1B), paired with all the other stimuli, resulting in a set of 120 unique trials. For a given trial, the two compound stimuli could differ anywhere from one to four cue dimensions, and this difference governed the underlying winning probabilities. That is, the probability that a left (*L*) or right (*R*) stimulus would win was determined based on the cue states comprising the left stimulus,  $C_L = \{c_{L,1}, c_{L,2}, c_{L,3}, c_{L,4}\}$ , and the right stimulus,  $C_R = \{c_{R,1}, c_{R,2}, c_{R,3}, c_{R,4}\}$ , and their associated weights,  $W_L = \{w_{c_{L,1}}, w_{c_{L,2}}, w_{c_{L,3}}, w_{c_{L,4}}\}$  and  $W_R = \{w_{c_{R,1}}, w_{c_{R,2}}, w_{c_{R,3}}, w_{c_{R,4}}\}$ :

$$P(L|C_L, C_R) = \frac{10 \sum_{i=1}^4 (w_{c_{L,i}} - w_{c_{R,i}})}{1 + 10 \sum_{i=1}^4 (w_{c_{L,i}} - w_{c_{R,i}})} \quad (1)$$

$$P(R|C_L, C_R) = 1 - P(L|C_L, C_R) \quad (2)$$

where *i* represents cue dimension (Table 1). Based on Eqs. (1) and (2), the winning stimulus was determined probabilistically on a trial-by-trial basis, and the outcome was signaled to the participant by presenting the words “win” or “lose” on the screen as post-decision feedback (Oh et al., 2016).

### 2.4. Procedure

On each trial, participants were presented with two compound stimuli and asked to indicate their choice via keypress within a specified choice window (Fig. 1A). Upon the choice deadline, stimuli disappeared from the screen, and the outcome of the choice (“win”, “lose”) or a no-response warning (“miss”) was displayed for 500 ms. After a variable intertrial interval (ITI) of 3–5 s drawn from a pseudo-exponential distribution (mean ITI = 3.5 s), the next trial began with a new pair of stimuli. Prior to the scan, all participants completed a 240 trial learning phase, comprised of two successive sets of all unique trials presented in random order. During the learning phase, participants were given a 1.5 s choice window to register their responses. The goal of this phase was to allow participants to explore and learn the cue weights by trial and error and familiarize themselves with the probabilistic classification task. Once the initial learning phase was complete, participants performed two more

**Table 1**  
Cue weight assignment.

Cue dimension $c_i$	Cue state 1 $w_{1,i}$	Cue state 2 $w_{2,i}$	Net cue weight $w_{net,i} = w_{1,i} - w_{2,i}$
$c_1$	0.9	0.1	0.8
$c_2$	0.8	0.2	0.6
$c_3$	0.7	0.3	0.4
$c_4$	0.6	0.4	0.2

Net weights indicate the relative importance of each cue dimension in determining the positive outcome in a given stimulus pair.

task phases (240 trials/phase) inside the scanner: (1) a low time pressure (LowP) phase with 1.5 s choice window (identical to the practice phase), and (2) a high time pressure (HighP) phase with a 0.5 s choice window. Each phase was separated into four runs (60 trials/run).

### 2.5. Behavioral performance analysis

Data analyses were based on optimal choices favored by the probability of winning (Eqs. (1) and (2)), independent of the probabilistic outcome provided to participants. In other words, a decision was considered correct when a participant chose a stimulus with the larger sum of weights. For the purpose of evaluating behavioral performance (% correct choices), trials with two stimuli that had an equal sum of weights were excluded since a correct choice cannot be defined, i.e.,  $P(L|C_L, C_R) = P(R|C_L, C_R) = 0.5$ . In reporting analysis of variance (ANOVA) measures, violations of sphericity assumptions were corrected by Greenhouse-Geisser correction to the degrees of freedom. Similarly, in reporting *t*-test results, degrees of freedom were corrected for unequal variance where necessary.

#### 2.5.1. Sum of evidence (SoE)

To formally define the objective difficulty of reaching the correct decision for a given trial, we computed each trial's SoE, the sum of available evidence,  $|\sum_{i=1}^4 (w_{c_{L,i}} - w_{c_{R,i}})|$ , which is equivalent to the absolute value of log odds that the left (or right) stimulus will be the one yielding a positive outcome. The inner term of the SoE equation corresponds to a decision variable, where, ideally, the subject is assumed to choose left, when  $\sum_{i=1}^4 (w_{c_{L,i}} - w_{c_{R,i}}) > 0$ , and right, when  $\sum_{i=1}^4 (w_{c_{L,i}} - w_{c_{R,i}}) < 0$ . Hence, as the magnitude of SoE decreases, the decision becomes more difficult, which is also associated with an increasing uncertainty of observing a positive outcome. For the SoE analyses, performance was analyzed by sorting trials based solely on the magnitude of SoE and therefore, different combinations of cues that share the same SoE were categorized as the same type of event. This resulted in 11 SoE levels, ranging from 0 (no evidence,  $P(L|C_L, C_R) = P(R|C_L, C_R) = 0.5$ ) to 2 (maximum available evidence, e.g.,  $P(L|C_L, C_R) = 0.99$ ). In addition to the objectively defined amount of evidence, we also quantified the *subjective* SoE on each trial using the sum of inferred cue weights,  $w^*$  (see below), under low and high time pressure conditions. Like the objective SoE, subjective SoE is closely related to perceived decision difficulty of a given trial. For the behavioral data analyses, we employed SoE as a basic manipulation check, by testing whether % correct choices and response times scale with SoE. In the neuroimaging analyses, we employed both subjective and objective SoE to probe which brain regions tracked the amount of evidence or outcome uncertainty, tailored to each participant's decision strategy under low and high time pressure (detailed below).

#### 2.5.2. Subjective cue weights

To characterize the decision strategies participants employed in the LowP and HighP phases, we focused our analyses on quantifying the degree to which each cue dimension affected participants' choices. To this end, we performed logistic regression using variational Bayesian inference (Drugowitsch, 2013; Oh et al., 2016). We first defined an optimal strategy model,  $Model_{opt}$ , which assumes that participants utilized all four cue dimensions to guide their choices. Then, for each participant per phase, we constructed an  $N$  (total number of trials)  $\times$  4 (number of cue dimensions) input matrix,  $x_{opt}$ , coding for the sign of cue dimension differences on each trial, i.e., 0 for  $w_{c_{L,i}} = w_{c_{R,i}}$ , 1 for  $w_{c_{L,i}} > w_{c_{R,i}}$ , and  $-1$  for  $w_{c_{L,i}} < w_{c_{R,i}}$  for a given cue dimension *i*. Logistic regression was performed based on  $x_{opt}$ , which returned parameters of a fitted logit model,  $w_{opt}$ , and a lower bound of the marginalized log-likelihood,  $P(D|Model_{opt})$ , of the observed choice data,  $D$ :

$$P(\text{choice} = L | x_{opt}, w_{opt}) = \frac{1}{1 + e^{-(w_0 + x_{opt} \times w_{opt})}} \quad (3)$$

$$P(w_{opt} | \alpha_{opt}) = \mathcal{N}(w_{opt} | 0, \alpha_{opt}^{-1} I) \quad (4)$$

$$P(\alpha_{opt}) = \text{Gamma}(\alpha_{opt} | a_0, b_0) \quad (5)$$

with  $w_0$  representing a  $N \times 1$  vector for estimating the intercept. Hyper priors ( $a_0 = 0.345$  and  $b_0 = 0.584$ ) were chosen based on the posterior distributions of the weights computed from the initial learning phase in line with an empirical Bayesian approach (for additional details, see Oh et al., 2016). Then, subjective cue weights,  $w^*$ , were calculated by transforming the fitted coefficients,  $w_{opt}$ , to log base 10:

$$w^* = w_{opt} \times \log_{10} e \quad (6)$$

In contrast to the net weights corresponding to the objective importance of each cue dimension (Table 1), subjective cue weights highlight the perceived importance of each cue dimension for each subject. Since the magnitude of subjective cue weights roughly corresponds to decision noise, a subject can be considered relatively optimal when their subjective weights are perfectly correlated with the true net weights described in Table 1.

### 2.5.3. Comparison between decision strategies adopted under low and high time pressure

To identify the cue dimensions that were effectively used during each phase, we further expanded our model space and explored a large set of plausible decision strategy models, accounting for every possible combinations of cue usage including the optimal model defined above (Fig. 2D). For a given model  $m$  ( $m = 1, \dots, 14, opt$ ), an input matrix,  $x_m$ , was constructed using cue dimensions that were included in the model, which then was used to compute  $P(D | Model_m)$  based on Eqs. (3)–(5). We compared 15 different decision strategy models to identify the most likely cue usage under conditions of low and high time pressure. The optimal model represents a compensatory strategy model where participants were assumed to integrate all four cue dimensions in making their choices, whereas models 1 through 14 consisted of different variations of sub-optimal cue weight integration. To characterize decision strategies at the group level, we employed a Bayesian model selection procedure by submitting the log model evidences obtained from the variational Bayesian inference above (Rigoux et al., 2014; Stephan et al., 2009). This approach fits the hierarchical model by treating models as random effects that could vary across subjects, and estimates exceedance probabilities, which reflect the belief that a model,  $m$ , is more likely than any other model, given the marginalized likelihoods. The Bayesian model selection results reported here were calculated using the `spm_BMS` routine of the SPM12 software suite (<http://www.fil.ion.ucl.ac.uk/spm/software/spm12/>). Note that using relatively uninformative hyper priors ( $a_0 = 0.01$  and  $b_0 = 0.0001$ ) in Eq. (5) does not change the overall results of model comparison.

### 2.6. fMRI data acquisition

Images were acquired on a 3 T GE MR750 scanner. T1-weighted structural images were scanned parallel to the AC-PC plane (146 slices, slice thickness = 1 mm, TR = 8.124 ms, FoV = 256 mm  $\times$  256 mm, in-plane resolution = 1 mm  $\times$  1 mm). Functional images were scanned using a T2\*-weighted single-shot gradient EPI sequence (42 slices, slice thickness = 3 mm, TR = 2 s, TE = 28 ms, flip angle = 90°, FoV = 192 mm  $\times$  192 mm, in-plane resolution = 3 mm  $\times$  3 mm). 169 functional images per run were acquired for the first four runs of the LowP phase and 139 images per run were acquired for the last four runs of the HighP phase.

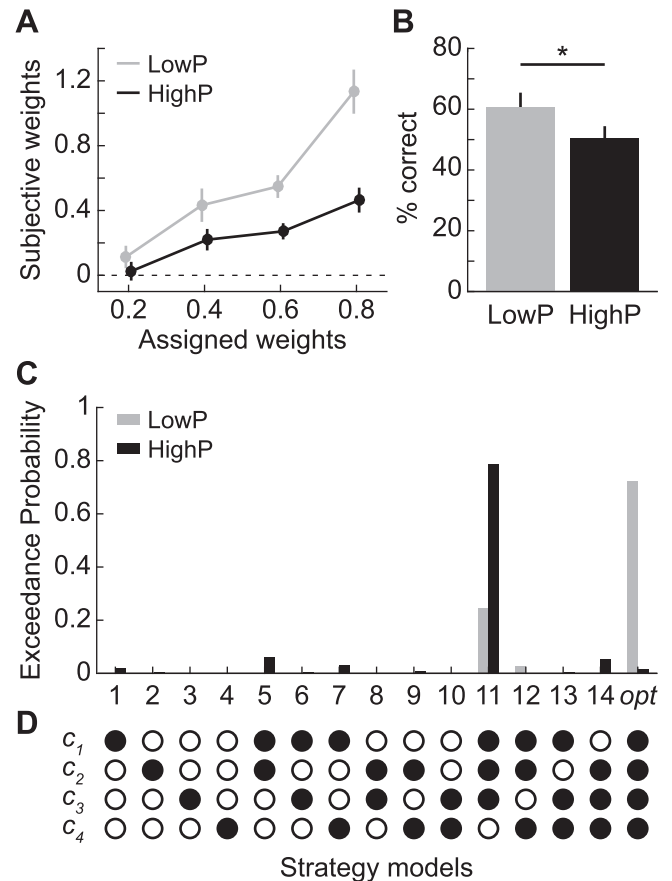


**Fig. 2.** Subjective cue weights and strategy model selection. **A**, Average subjective cue weights as a function of objective, pre-assigned cue weights. Participants learned and utilized the correct relative rankings of the cues in both experimental phases. **B–D**, Bayesian model selection results from comparing **D**, decision models covering every possible cue usage. Filled circles (●) denote the cue dimensions that are included in a given model. **C**, Exceedance probabilities of each strategy model under low and high time pressure conditions. Under low time pressure (LowP), the optimal model (Model *opt*) was the most likely model. Under high time pressure (HighP), participants shifted to employing a satisficing decision strategy by utilizing only the three highest-weighted cues and ignoring the least important one (Model 11). **B**, Percentage of correct choices when only the least important cue is different between the stimulus pair. Error bars indicate SEM; \* $p < 0.01$ .

### 2.7. Image preprocessing

Preprocessing and univariate statistical analyses were performed using SPM12 (<http://www.fil.ion.ucl.ac.uk/spm/software/spm12/>). After discarding the first four scans of each run, functional images were realigned to their mean image and corrected for slice timing. Each participant's structural image was co-registered to the mean functional image and segmented into gray matter, white matter, cerebro-spinal fluid, bone, soft tissue, and air/background. The deformation field map obtained through segmentation was applied to normalize the subject's functional images to the Montreal Neurological Institute (MNI) template space. Functional images were resampled into 3  $\times$  3  $\times$  3 mm voxel size and spatially smoothed with a Gaussian kernel of 5 mm full-width at half maximum (FWHM).

### 2.8. fMRI data analyses

Assuming that participants learned the cue structure and associated weights, the decision task can be approached in two distinct but complementary (and not mutually exclusive) ways: (1) analyzing each cue dimension difference between the two compound stimuli present on a given trial based on *subjective cue weights*, and adding them up, and/or (2)

summing the cue states comprising each compound stimulus and estimating the difference between the sums of the two stimuli, which is also equivalent to the *subjective SoE*. Both approaches would lead to the same solution, with the first approach having more emphasis on parsing the compound stimuli out into individual cue dimension differences prior to integrating the cues to evaluate the total amount of evidence. The preferential use of either of these two approaches might depend on a participant's subjective cue weight distribution (e.g., weights are evenly distributed or one cue weight dominates all others) as well as on trial type (i.e., which cue dimensions differed between stimuli on a given trial). We assumed that participants likely used a mixture of these approaches, and we therefore focused our fMRI analyses on characterizing neural substrates of both subjective cue weight and SoE representation as a function of time pressure. For the following fMRI analyses, we used objectively correct trials (as favored by the probability defined in Eq. (1) and (2)) as the events of interest.

### 2.8.1. Neural representation of subjective cue weights

To identify brain regions that represent information about subjective cue weights of individual cue dimensions, we employed a multivariate decoding technique based on support vector machine regression (SVR). Recall that these analyses solely concern the informational value of the cues, rather than specific visual cue features, as our task design dissociated cue weights from specific cue dimensions/features across the subject population. To achieve maximal sensitivity, we used realigned and slice time corrected functional images in each participant's native space without spatial normalization and smoothing. Functional data were first analyzed using the standard general linear model (GLM) approach (Friston et al., 1994) to regress the BOLD signal against task models and to estimate parameter  $\beta$ s for conditions of interest. Four regressors, each representing a unique cue dimension, tracked the presence of the corresponding cue dimension difference between a compound stimulus pair on each trial. For example, if two stimuli were different in  $c_1$  and  $c_2$  dimensions but not in  $c_3$  and  $c_4$  on trial  $t$ , boxcar functions were created at trial  $t$  only in the regressors for  $c_1$  and  $c_2$ . Following this rule, all correct trials were modeled as boxcar functions of durations 2 s (LowP) or 1 s (HighP) aligned to trial onsets, capturing both the stimulus presentation and the subsequent feedback in each phase. As regressors of no interest, we included a categorical regressor of win (1) and lose (−1) probabilistic feedback. To account for differences in response time (RT) across trials and experimental phases, a parametric regressor of RT aligned to the trial onsets was also included. In addition, incorrect trials and trials with no response were modeled separately, along with six head-motion parameters and grand means of each run. All regressors were convolved with the canonical hemodynamic response function. The resulting parameter estimates of the four cue dimension regressors,  $\beta_{c_i}$  ( $i = 1, 2, 3, 4$ ), were used to search for brain areas that contain information about the subjective cue weights under low and high time pressure conditions.

Specifically, we conducted multivoxel pattern analysis (MVPA) with a whole-brain searchlight approach (Haynes et al., 2007; Kriegeskorte et al., 2006) that scanned through spheres of gray matter voxels (searchlight radius = 4 voxels) identified using each participant's gray matter mask produced from T1 segmentation. The MVPA was performed by using a linear SVR with a constant regularization parameter of  $C = 1$  (Kahnt et al., 2011), implemented in MATLAB. We iteratively used 3 of the 4 runs to train an SVR model and then used the remaining run as the test data set to predict the value of the subjective cue weights (i.e., a leave-one-run-out procedure). Prediction accuracy was determined by the Fisher's Z-transformed correlation coefficients (Kahnt et al., 2011) between the predicted values and the subjective cue weights,  $w^*$ , of the test data set. An accuracy map was constructed by averaging the prediction accuracy from 4-fold cross-validation for each center voxel of the searchlight spheres. We conducted the decoding analyses separately for the LowP and HighP phases, using the corresponding subjective cue weights.

The accuracy maps of each participant were normalized into the template MNI space and smoothed with a Gaussian kernel (FWHM = 5 mm) to account for differences in activation localization across subjects (Kahnt et al., 2011). The group analysis was performed by entering the accuracy maps into one-sample  $t$ -tests, separately for LowP and HighP phases. The  $p$ -value maps were corrected for multiple comparison using the CorrClusTh.m function developed for use with SPM (<http://www2.warwick.ac.uk/fac/sci/statistics/staff/academic-research/nichols/scripts/spm/spm8/corrclusth.m>), which determined that an uncorrected voxelwise threshold of  $p < 0.005$  combined with a cluster size of 46 voxels corresponded to cluster level corrected threshold of  $p < 0.05$ .

### 2.8.2. Modulation of neural activity by SoE

Subjective SoE reflects the integrated sum of subjective cue weights of a given trial, which should be highly correlated with the objective amount of evidence and decision difficulty. Therefore, brain regions modulated by subjective SoE likely encode not only the integrated sum of cue weights but also decision processes involved in producing a final choice output. Since subjective SoE can vary over up to 40 distinct levels, it would not yield a sufficiently reliable estimation of parameter  $\beta$ s (~5 trials/level) to utilize the multivariate analysis approach carried out on the subjective cue weights above (see *Neural representation of subjective cue weights*). Therefore, we instead employed a parametric modulation analysis within the standard mass-univariate GLM approach to detect areas whose activation was modulated by SoE. Correct trials were modeled as boxcar functions of 2 s (LowP) or 1 s (HighP) duration, aligned to trial onsets. A parametric regressor of subjective SoE, estimated separately for the LowP and HighP phases using the associated subjective weights, was attached to trial onsets. As the regressors of no interest, a categorical feedback regressor and a parametric regressor of RT were aligned to trial onsets. In addition, incorrect trials, trials with no response, six head-motion parameters, and grand means of each run were also included as regressors of no interest. All regressors were convolved with the canonical hemodynamic response function and regressed against the BOLD signal in each voxel. Within-subject effects of modulation of neural activity by subjective SoE were assessed for the LowP and HighP phases separately. The resulting single-subject contrast maps were entered into group-level analyses, which treated subjects as random effects.

To probe for differences between experimental conditions, we further contrasted effects of SoE modulation between the LowP and HighP phases. For all analyses, the  $p$ -value maps were corrected for multiple comparison using the function CorrClusTh.m, which determined that an uncorrected voxelwise threshold of  $p < 0.005$  combined with a cluster size 96 to 105 voxels ensured a false discovery rate  $< 0.05$ . In addition, although SPM orthogonalizes parametric modulators to compute the GLM, results could potentially be influenced by the order of the modulators. To ensure that the observed effects are independent from this influence, we additionally ran GLMs by varying the order of parametric regressors (subjective SoE, feedback, and RT), which did not yield any significant difference in overall neuroimaging results.

### 2.8.3. Region-of-interest analysis of objective SoE

To further investigate the relationship between neural encoding of objective and subjective SoE, we performed a region-of-interest (ROI) analysis. First, we identified brain regions modulated by subjective SoE in both low and high time pressure phases by applying a “logical AND” conjunction analysis (Nichols et al., 2005). Voxels that passed the multiple comparison correction in both the LowP and HighP phases were included in the conjunction map. For clusters that span multiple regions, we applied anatomical masks to include only the voxels within a specified area. Anatomical ROIs were defined using the WFU PickAtlas toolbox (Maldjian et al., 2004, 2003) and clusters with less than 10 voxels were excluded from the analysis. Then, we employed the same GLM approach as above but treated each objective SoE level as a separate

condition. To roughly match the number of trials included in each regressor, we merged the three highest SoE levels (1.6, 1.8, 2), which resulted in nine parameter estimates  $\beta_{SoE_i}$  with  $i$  ranging from 0 (no evidence) to  $1.6^*$  (high evidence). Similar to the previous GLMs, correct trials corresponding to each SoE level were modelled with boxcar functions along with parametric modulators of feedback and RT. Additionally, incorrect trials, trials with no response, six head-motion parameters, and grand means of each run were included. To investigate the effect of objective SoE on modulating activities in regions sensitive to subjective SoE, the parameter estimates obtained from the GLM were extracted and averaged within each ROI, and tested for linear trend using a repeated-measure ANOVA.

#### 2.8.4. Practice effect analysis

Since participants completed the low and high time pressure phases in a block-wise, sequential manner, it is important to rule out that changes in BOLD signal across experimental phases are not merely driven by task practice. Therefore, we conducted an additional GLM analysis to examine the presence of neural practice effects. Specifically, we hypothesized that we would observe gradual BOLD signal changes over time if practice effects were present. To characterize overall changes in trial-induced BOLD activation over the course of the experiment, we divided our task into four different sets (120 trials/set, 2 sets/phase), each consisting of a complete set of unique stimulus combinations. Then, correct trials were modeled as boxcar functions of 2 s (LowP) or 1 s (HighP) duration, aligned to trial onsets, with parametric regressors of feedback and RT. Additionally, incorrect trials, trials with no response, six head-motion parameters, and grand means of each run were included as regressors of no interest. All regressors were convolved with the canonical hemodynamic response function. Then, the percent signal changes (MarsBaR; <http://marsbar.sourceforge.net/>) and the parameter estimates,  $\beta_{Trial}$ , were extracted and averaged within the predefined ROIs and entered into  $2 \text{ (sets)} \times 2 \text{ (LowP/HighP phases)}$  repeated-measures ANOVAs. To further investigate changes in subjective SoE modulation per set, we repeated the same GLM analysis using subjective SoE (see above), but splitting the data into four sets instead of two phases.

### 3. Results

#### 3.1. Behavioral data

##### 3.1.1. Task performance

Participants performed a multi-cue probabilistic classification task under low (1500 ms) and high (500 ms) time pressure inside the fMRI scanner. Their task was to compare two compound stimuli comprised of four different visual features (color, shape, contour, and line orientation) and make a prediction as to which stimulus is more likely to win (Fig. 1A and B). Upon each choice deadline, the outcome (“win” or “lose”), determined probabilistically based on the cue weights, was displayed (Table 1; see Materials and Methods). Performance was evaluated based on the number of correct choices favored by the cue weights, independent of the probabilistic outcome feedback participants experienced. Throughout the learning phase prior to the scan, participants were able to gradually improve their decision performance as characterized by a significant main effect of run (accuracy:  $F_{(3,72)} = 8.36, p < 0.001$ ; RT:  $F_{(3,72)} = 7.54, p = 0.001$ ) and a linear trend (accuracy:  $F_{(1,24)} = 14.52, p = 0.001$ ; RT:  $F_{(1,24)} = 9.80, p = 0.005$ ) (Fig. 1C left). In the LowP phase (1500 ms response window), participants achieved better mean decision accuracy,  $t_{24} = 5.62, p < 0.001$ , and expedited decision speed,  $t_{24} = 4.12, p < 0.001$ , compared to the learning phase as they became yet more accustomed to the task, but performance remained stable throughout the LowP phase (main effect of run, accuracy:  $F_{(3,72)} = 0.70, p = 0.56$ ; RT:  $F_{(3,72)} = 2.66, p = 0.06$ ) (Fig. 1C middle). Note that the marginal effect on RT was not due to a linear increase in response speed over time, and is therefore unlikely to reflect continued

learning in the LowP phase (see Table 2 for run-wise descriptive statistics). In addition, performance scaled with objective SoE, defined by the sum of cue weight differences between the stimulus pair. As SoE increased, percent correct choices increased (linear trend,  $F_{(1,24)} = 153.03, p < 0.001$ ) and decision time decreased (linear trend,  $F_{(1,24)} = 30.54, p < 0.001$ ), indicating that participants learned to integrate the predictive value of the four cue dimensions to base their decisions on (Fig. 1D and E).

As anticipated, increased time pressure in the HighP phase (500 ms response window) speeded up decision time,  $t_{24} = 20.86, p < 0.001$ , compared to the LowP phase, but had a detrimental effect on decision making, revealed by a large decrease in accuracy,  $t_{24} = 8.08, p < 0.001$ , which remained constant throughout the HighP phase (main effect of run, accuracy:  $F_{(3,72)} = 1.53, p = 0.21$ ; RT:  $F_{(3,72)} = 0.62, p = 0.56$ ) (Fig. 1C right). Despite this significant decrement in overall performance, decision accuracy nevertheless scaled with objective SoE in the HighP phase (linear trend,  $F_{(1,24)} = 30.54, p < 0.001$ ), confirming that participants were able to use available cue information to guide their choices (Fig. 1D). By contrast, RT was no longer related to SoE (linear trend,  $F_{(1,24)} = 0.96, p = 0.34$ ), presumably due to the severe time pressure enforced in this condition (Fig. 1E).

##### 3.1.2. Subjective cue weights

To examine the relative importance of each cue dimension in guiding participants' choices, separate sets of subjective cue weights for the LowP and HighP phases were obtained using logistic regression (Fig. 2A, Eqs. (3)–(6)). A repeated-measures ANOVA revealed a main effect of cue weights,  $F_{(3,72)} = 21.29, p < 0.001$ , which was characterized by a significant linear trend,  $F_{(1,24)} = 39.02, p < 0.001$ , indicating that participants were able to correctly rank the cues according to their objective order of importance, which was true for both the LowP,  $F_{(3,72)} = 23.55, p < 0.001$ , and the HighP,  $F_{(3,72)} = 8.86, p < 0.001$ , phases. Nevertheless, the main effect of phase was significant,  $F_{(1,24)} = 38.71, p < 0.001$ , as subjective cue weights were overall smaller in the HighP than in the LowP phase, reflecting a general down-weighting of cue weights under time pressure. Since the magnitude of fitted weights also corresponds to the decision noise, this overall decrease of cue weights reflects the deterioration of decision making performance in the HighP phase. Finally, the phase  $\times$  cue weight interaction,  $F_{(3,72)} = 11.23, p < 0.001$ , was also significant, as the relative difference between cue weights between the two phases increased as a function of the assigned cue weights.

##### 3.1.3. Decision strategy model selection

To characterize the difference in decision strategy under the conditions of low and high time pressure, we explored 15 different plausible strategy models covering every possible combinations of cue usage (Fig. 2D). We estimated marginalized log-likelihood by fitting a logistic function using variational Bayesian inference (Eqs. (3)–(5); Drugowitsch, 2013) for each model per participant. These log model evidences were then used to fit the hierarchical model (Rigoux et al., 2014; Stephan et al., 2009) to estimate the most likely strategy model employed in each experimental phase at the group level (Fig. 2C). In the LowP phase, the optimal cue integration model was the most likely model with an exceedance probability of 0.72. In the HighP phase, however, Model 11, which utilizes only the three most informative cues, was the winning model, with an exceedance probability of 0.79. This shift in strategy from the optimal model to Model 11 suggests that participants dropped the worst cue in their decision-making process under increasing time pressure, replicating our previous results (Oh et al., 2016). Additionally, to address the possibility that participants may have engaged in a stimulus-based decision process by learning and memorizing weights of each of the 16 compound stimuli rather than the four cue dimensions, we also included a strategy model based on summed cue weights in the model comparison with the other 15 aforementioned cue-based models per phase. The group-level model comparison results yielded very weak

support for the stimulus-based model in all three phases (exceedance probabilities <0.005), suggesting that participants engaged in a cue dimension-based decision process, regardless of time pressure.

To further investigate whether this shift in strategy was simply due to running out of time to integrate all cues under severe time pressure, rather than due to a strategic neglect of the weakest cue, we examined performance on trials when only the least important cue,  $c_4$ , was different between the stimulus pair. Given the visual saliency of only one cue differing between the two stimuli, and the fact that only that one cue ( $c_4$ ) had to be evaluated in these trials, we would not expect a participant to run out of time in this condition. However, as shown in Fig. 2B, the difference in choice accuracy between the LowP and HighP phases was significant,  $t_{24} = 2.86, p = 0.009$ , with HighP phase performance not differing significantly from chance,  $t_{24} = 0.13, p = 0.90$ . Moreover, decision accuracy in the LowP phase was 60.75%, which was significantly greater than chance,  $t_{24} = 2.29, p = 0.03$ . Given that the probability of receiving “win” feedback in this condition, if a correct choice is made, is 0.61 (see Eq. (1)), this observation is in line with probability matching behavior, as shown in a number of previous studies (see e.g., Vulkan, 2000). In sum, these results further support the conclusion that the shift in cue usage was a strategic choice of participants to restrict their search space and therefore to integrate less cues to arrive at good-enough decisions under severe time pressure. Having established that time pressure produced noisier decisions and a dropping of the weakest cue, we turned to ask how these changes in decision making are reflected in brain activity.

### 3.2. Neuroimaging data

#### 3.2.1. Neural representation of subjective cue weights

Once participants have formed an understanding of the cue structure, one way to effectively solve the classification task is to compare a given compound stimulus pair and extrapolate the differences in cue dimensions using subjective cue weights. Then, one can use this cue information to arrive at a final choice directly (e.g., when one cue out-

weighs the rest of available cue(s) or sum the weights to arrive at the (subjective) SoE. Hence, this process requires breaking down compound stimuli into individual cue dimensions and weighting them appropriately, which serves as a precursor to the estimation of subjective SoE and/or a final choice output. Therefore, we first sought to examine which brain regions contained information about the subjective importance of each cue dimension in solving the classification task. We employed a whole-brain searchlight SVR to find BOLD patterns that are significantly predictive of the magnitude of subjective cue weights in each experimental phase. As our behavioral data suggest, participants used varying decision strategies under low and high time pressure, with increased decision noise and a reduced information search space under high pressure. This change is represented by relative over-weighting of the cues that each participant deemed important and down-weighting the cues that are considered less informative (Fig. 2A). Therefore, to account for large individual differences in cue usage, we focused our neuroimaging analyses on using subject- and phase-specific subjective cue weights (or the sum of weights represented by subjective SoE; see below), rather than fixed objective cue weights, to achieve higher sensitivity in detecting brain regions that encode decision evidence. Hence, our decoding approach using a linear SVR aimed to delineate the brain regions that are associated with the subjective evaluation of individual cue dimensions under each experimental condition.

The results are summarized in Fig. 3 and Table 3 ( $p < 0.05$ , corrected). Under low time pressure, subjective cue weights could be successfully decoded from neural signals in the dorsal striatum, dorsolateral prefrontal cortex (dlPFC), posterior cingulate cortex (PCC), and precuneus (Fig. 3A). Under increased time pressure, however, above-chance decoding of cue weight information was found in the postcentral gyrus and cerebellum (Fig. 3B). Furthermore, there were significant differences in decoding accuracies between task phases in the dorsal striatum ( $t_{24} = 3.26, p = 0.003$ ), dlPFC ( $t_{24} = 2.45, p = 0.02$ ), and PCC ( $t_{24} = 4.45, p < 0.001$ ), indicating deterioration in individual cue weight information in these clusters under increased time pressure (Fig. 3C). Interestingly, we found significantly enhanced encoding of cue

**Table 2**  
Decision accuracy (%) and response time (ms) across task runs.

Run	Learning				Low time pressure				High time pressure			
	1	2	3	4	5	6	7	8	9	10	11	12
Accuracy (%)	60.9 (2.4)	65.7 (1.8)	69.9 (2.1)	69.9 (2.3)	76.3 (2.3)	74.0 (1.9)	74.9 (2.2)	76.6 (2.0)	62.0 (2.2)	58.4 (2.3)	61.0 (2.3)	62.1 (2.1)
RT (ms)	884 (29)	843 (28)	804 (29)	816 (30)	751 (23)	738 (22)	714 (22)	727 (20)	366 (5)	370 (5)	370 (6)	367 (7)

Numbers in parenthesis are standard error of the mean (SEM).

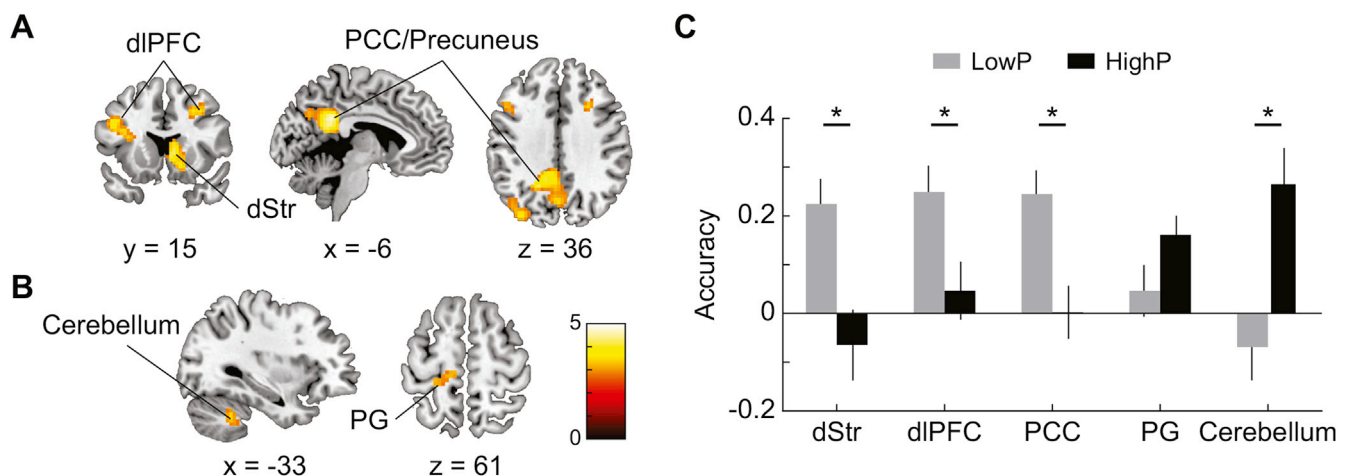


**Fig. 3.** Neural representation of subjective cue weights. **A-B,** Brain regions containing fMRI patterns significantly predictive of subjective cue weights under **A,** low time pressure, and **B,** high time pressure ( $p < 0.05$ , corrected). Image display according to neurological convention (left is left). **C,** Average prediction accuracy (Fisher's Z-transformed correlation coefficients) of each cluster. Accuracy of zero represents at chance decoding performance. dStr = dorsal striatum; PG = postcentral gyrus; Error bars indicate SEM; \* $p < 0.05$ .

**Table 3**  
Clusters showing significant decoding accuracy of subjective cue weights.

Region	Hemisphere	Peak MNI (x, y, z)	Peak <i>t</i>	Cluster size (searchlights)
<b>Low time pressure</b>				
Precuneus/posterior cingulate	L/R	(−6, −46, 29)	4.73	1,219
Caudate/putamen	R	(9, 14, 2)	4.29	160
Middle/inferior frontal gyrus	L	(−45, 17, 29)	4.07	108
Middle frontal gyrus	R	(27, 17 38)	4.00	86
<b>High time pressure</b>				
Postcentral/medial frontal gyrus	L	(−12, −25, 59)	3.58	65
Cerebellum	L	(−33, −49, −37)	3.45	66

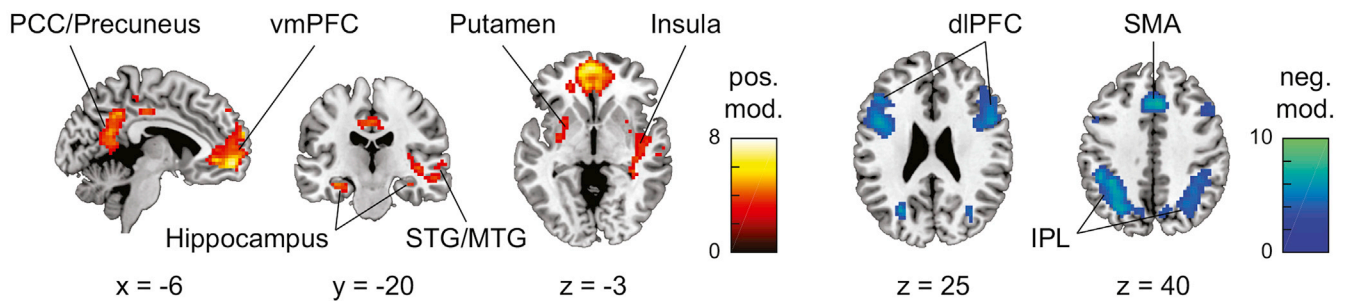
information in the cerebellum in the HighP phase ( $t_{24} = 3.84, p < 0.001$ ). Thus, in line with deterioration in behavioral decision making and down-weighting of subjective cue weights, encoding of individual cue weight information in fronto-parietal and striatal regions under low pressure was dampened under high pressure. Note that the results remain consistent over variations of the regularization parameter, *C*, in SVR. We

next turned to interrogating how this loss of fidelity of subjective cue weight representations for specific cue dimensions may be accompanied by changes in the neural encoding of the SoE or decision variable.

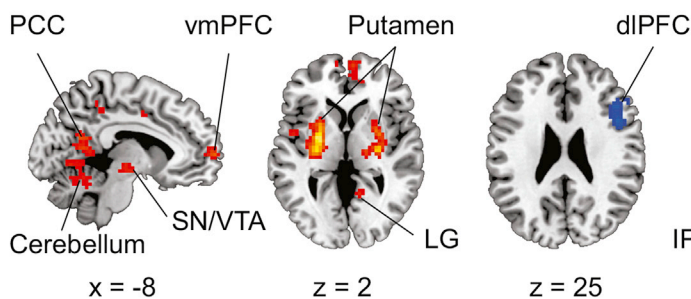
**3.2.2. Modulation of neural activity by SoE**

The magnitude of SoE represents the log odds of observing a positive

**A Low time pressure**



**B High time pressure**



**C HighP > LowP**

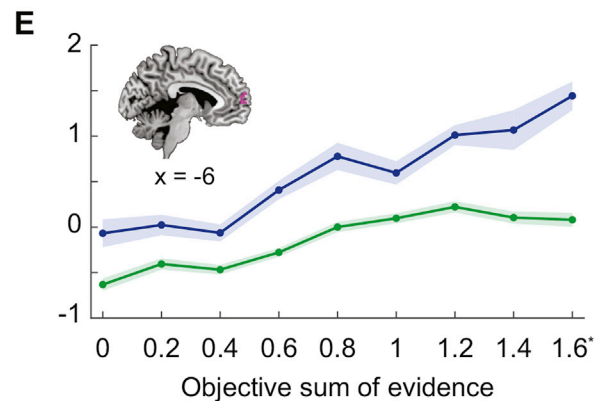
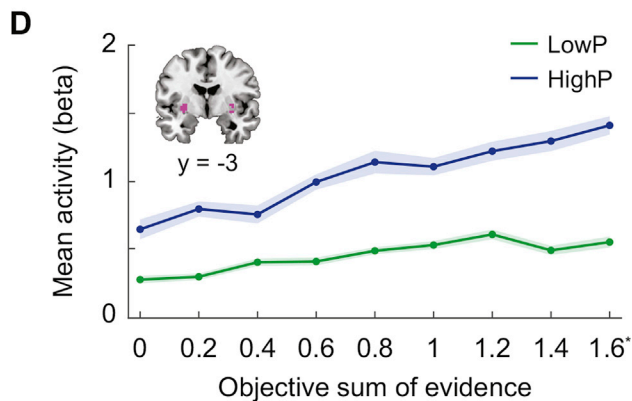
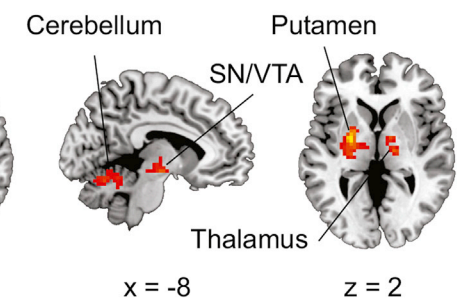


**Fig. 4.** Modulation of neural activity by SoE. A-C, Brain regions significantly modulated by *subjective* SoE under A, low time pressure and B, high time pressure. Positive modulation (red) indicates activity increasing with accumulation of evidence, whereas negative modulation (blue) represents activity increasing with decreasing SoE, and hence, greater uncertainty or decision difficulty. C, Brain areas demonstrating significantly greater positive SoE modulation in the HighP compared to the LowP phase. STG = superior temporal gyrus; MTG = middle temporal gyrus; LG = lingual gyrus. All maps were whole-brain corrected to  $p < 0.05$ . D-E, Mean activity as a function of *objective* SoE in the D, putamen, and E, vmPFC. Both clusters demonstrate significantly positive linear trend in the LowP and HighP phases. Objective SoE of 1.6\* includes trials with SoE levels ranging from 1.6 to 2. Shaded area indicates SEM.

**Table 4**  
Activation clusters for positive subjective SoE modulation.

Region	Hemisphere	Peak MNI (x, y, z)	Peak t	Cluster size (voxels)
Low time pressure				
Medial frontal gyrus/anterior cingulate	L/R	(−6, 56, −7)	7.33	725
Precuneus/posterior cingulate	L/R	(−9, −52, 38)	5.86	308
Superior/middle temporal gyrus/insula/hippocampus/putamen	R	(54, −28, 14)	5.66	771
Superior/middle frontal gyrus	L	(−12, 47, 41)	5.35	155
Superior/middle temporal gyrus/insula	L	(−60, −58, 20)	5.25	388
Parahippocampal gyrus/putamen/hippocampus	L	(−33, −19, −16)	4.60	107
Cingulate gyrus	L	(−9, −25, 41)	4.74	117
Cuneus	R	(18, −85, 20)	4.39	111
High time pressure				
Putamen/insula/parahippocampal gyrus/midbrain/cerebellum	L	(−27, −4, 2)	6.87	1,088
Putamen/insula/parahippocampal gyrus	R	(30, −16, 5)	5.51	389
Posterior cingulate	L	(−12, −58, 14)	5.04	113
Postcentral/precentral gyrus/precuneus	L/R	(27, −52, 62)	4.76	377
Posterior cingulate/lingual gyrus/cerebellum	R	(15, −55, 11)	4.66	199
Medial frontal gyrus	L/R	(−9, 65, 5)	4.35	103
Supplementary motor area	L/R	(−3, −13, 44)	4.34	99
Precentral/postcentral gyrus	R	(27, −25, 44)	3.92	96
High time pressure > low time pressure				
Cerebellum/lingual gyrus	L	(−24, −61, −22)	6.20	541
Putamen/thalamus	L	(−24, −4, 2)	5.76	241
Thalamus/midbrain	R	(18, −16, −1)	4.93	151

outcome from choosing either a left or right compound stimulus. Therefore, it represents the total amount of evidence available to a participant, which in turn, determines the objective difficulty of a given trial. That is, uncertainty of outcome increases with decreasing SoE, which makes decision-making more difficult. Similarly, subjective SoE reflects participants' perceived difficulty of a given trial. Thus, we hypothesized that brain regions modulated by SoE should encode both the integrated sum of cue weights and associated uncertainty/difficulty that produce the final choice output. Specifically, to account for individual variability in cue learning and decision strategies employed under low and high time pressure conditions, we sought to examine the areas modulated by *subjective* SoE, which was estimated using the sum of subjective weights of the cue dimension present on a given trial (see Materials and Methods). To this end, we employed the standard GLM approach using trial-by-trial subjective SoE as a parametric modulator.

The results are summarized in Fig. 4 and Tables 4 and 5 ( $p < 0.05$ , corrected). We found distinct sets of brain regions displaying either a positive modulation effect (Table 4), reflecting increasing activity with greater decision evidence and certainty, or a negative modulation effect (Table 5), where activity increased with greater decision difficulty and uncertainty (i.e., decreasing magnitude of SoE). In the LowP phase, positive scaling with SoE magnitude was found in the vmPFC, extending to the rostral anterior cingulate and superior frontal gyrus; in superior temporal gyrus, extending to the insula, putamen and hippocampus; and in precuneus and PCC (Fig. 4A, Table 4). By contrast, negative SoE modulation was found in the dlPFC, dorsal medial PFC, and lateral inferior parietal lobule (IPL) (Fig. 4A, Table 5), a set of regions that are commonly activated under high attentional demand and are often referred to as the fronto-parietal cognitive control network (Dosenbach et al., 2006; Duncan and Owen, 2000; Niendam et al., 2012; Wager et al.,

2004). Under increased time pressure, similar areas positively modulated by subjective SoE in the LowP condition were found, with more confined activation in the putamen, vmPFC, and PCC. In addition, areas related to motor control such as the supplementary motor area (SMA), cerebellum, precentral and postcentral gyrus also showed enhanced modulation (Fig. 4B, Table 4). Again, similar to the LowP phase, significant negative modulation effects were observed in the right dlPFC and IPL (Fig. 4B, Table 5), suggesting reduced engagement of the fronto-parietal control network when choices have to be made quickly under severe time pressure.

When testing for regions with similar response profiles across low and high time pressure by means of a conjunction analysis, positive modulation of SoE was commonly found in the putamen, vmPFC, PCC, precuneus, parahippocampal gyrus, and insula. Additionally, negative modulation of SoE was commonly observed in the dlPFC and IPL, suggesting a critical role of these regions associated with an accumulation of evidence or subjective confidence regardless of time pressure. Finally, and most importantly, to determine the way in which time pressure alters decision making in terms of the modulation of neural activity by decision evidence, we directly contrasted the modulation effect of subjective SoE between the LowP and HighP phases (Fig. 4C, Table 4). The results revealed a significantly *greater* positive modulation of activity by SoE in the putamen, thalamus, dopaminergic midbrain, and cerebellum during the HighP compared to the LowP phase. The midbrain cluster consisted of substantia nigra (SN, 83 voxels) and ventral tegmental area (VTA, 38 voxels), which were identified based on a probabilistic atlas (Murty et al., 2014). In sum, the results highlight enhanced sensitivity in the basal ganglia, thalamus, and cerebellum to decision-relevant evidence under high time pressure.

Since participants' performance scaled linearly with objective SoE

**Table 5**  
Activation clusters for negative subjective SoE modulation.

Region	Hemisphere	Peak MNI (x, y, z)	Peak t	Cluster size (voxels)
Low time pressure				
Medial frontal gyrus	L/R	(−3, 11, 50)	9.21	294
Middle/inferior frontal gyrus	L	(−45, 8, 29)	7.71	374
Inferior parietal lobule	L	(−36, −43, 38)	7.35	576
Middle/inferior frontal gyrus	R	(51, 23, 32)	5.88	387
Inferior parietal lobule	R	(36, −58, 47)	5.38	465
High time pressure				
Inferior parietal lobule	R	(33, −64, 41)	4.80	110
Middle/inferior frontal gyrus	R	(48, 29, 20)	4.59	99

(see Fig. 1D), we sought to examine whether the regions modulated by subjective SoE are similarly sensitive to objective SoE. That is, since objective and subjective SoEs are highly correlated, especially for high performers, we expected that similar regions would also be modulated by objective SoE. We conducted an additional ROI analysis based on the clusters sensitive to subjective SoE modulation identified through the conjunction analysis. We applied anatomical masks to separate clusters that span multiple areas, and clusters with more than 10 voxels were used for ROI analysis. This included the putamen (70 voxels), vmPFC (57 voxels), and PCC (59 voxels) from the positive SoE modulation effect, and the dlPFC (81 voxels) and IPL (84 voxels) from the negative SoE modulation effect. For both the low and high time pressure phases, parameter estimates,  $\beta_{\text{SoE}_i}$   $i = 0, \dots, 1.6^*$ ;  $\text{SoE} = 1.6^*$  includes trials from the three highest SoE levels, 1.6, 1.8, and 2), from all five regions showed highly significant linear trend as a function of objective SoE. Specifically, the putamen (LowP:  $F_{(1,24)} = 21.28, p < 0.001$ ; HighP:  $F_{(1,24)} = 19.73, p < 0.001$ ) (Fig. 4D), vmPFC (LowP:  $F_{(1,24)} = 20.63, p < 0.001$ ; HighP:  $F_{(1,24)} = 13.56, p = 0.001$ ) (Fig. 4E), and PCC (LowP:  $F_{(1,24)} = 21.47, p < 0.001$ ; HighP:  $F_{(1,24)} = 9.10, p = 0.006$ ) showed significantly positive linear relationship with objective SoE. Similarly, both the dlPFC (LowP:  $F_{(1,24)} = 13.97, p = 0.001$ ; HighP:  $F_{(1,24)} = 5.88, p = 0.02$ ) and IPL (LowP:  $F_{(1,24)} = 17.39, p < 0.001$ ; HighP:  $F_{(1,24)} = 9.03, p = 0.006$ ) demonstrated significantly negative linear relationship with objective SoE. The results suggest that these regions closely track the integrated sum of decision-relevant information on each trial at both subjective and objective level, regardless of time pressure.

Lastly, to ensure that our results were not simply driven by differences in RT profiles in the LowP and HighP phases, we conducted additional analyses. For all GLMs reported above, trial-by-trial RTs were modeled explicitly as a parametric modulator, and we found no significant differences in RT modulation across phases. Additionally, evidence accumulation models such as the drift diffusion model (e.g., Ratcliff, 1978) suggest that time pressure induces lowering of the decision bound, which would in turn result in a change in the magnitude of the subjective cue weights but not their ratios. To account for this prediction, we analyzed fMRI data using normalized subjective cue weights, and found no difference in results, both in the subjective cue weights (SVR) and the subjective SoE (parametric GLM) analyses. Therefore, it is highly unlikely that the phase differences in neural cue weight and SoE encoding reported above are merely reflective of RT differences between conditions.

Taken together, results from the SoE analysis showed that activity in the putamen, dopaminergic midbrain (SN/VTA), thalamus, and cerebellum is positively correlated with trial-by-trial variations in subjective SoE, and display a significantly greater sensitivity to the decision variable under severe time pressure than under low time pressure. Furthermore, regardless of time pressure, the putamen, vmPFC, and PCC were positively modulated by subjective SoE, whereas activity in the frontoparietal cognitive control network was consistently sensitive to decision uncertainty, characterized by negative SoE modulation. Additionally, we found that these areas also closely tracked objective SoE, confirming their role in encoding integrated decision-relevant information.

### 3.2.3. Ruling out practice effects

We performed the time pressure manipulation in a block-wise, sequential manner to avoid spillover effect of severe time pressure influencing decision behavior on subsequent low pressure blocks. This experimental design, however, raises a concern that changes in behavior and cortical activity across experimental phases we report could be influenced by task practice. At the behavioral level, practice effects are defined as an increase in accuracy and decrease in response time (Ashby et al., 2010; Kelly and Garavan, 2005; Schneider and Shiffrin, 1977). As reported in the previous section (see *Task performance*), both decision accuracy and RT remained constant within each the LowP and HighP

phase during the scan ( $ps > 0.05$ ). In addition, contrary to the assumption of improving performance with continued practice, we observed significant impairment in choice performance when moving from the low to high time pressure condition. Hence, behaviorally, our within- and between-phase observations do not support a practice effect hypothesis.

At the neural level, practice is usually associated with an overall decrease in BOLD activation of the cognitive control and attentional network (i.e., prefrontal and parietal areas) as the task becomes automatized (see Kelly and Garavan, 2005 for a review). Some studies, additionally, have reported enhanced post-learning subcortical processing (Doyon et al., 2009; Lehericy et al., 2005; Van Turennout et al., 2003), although the results are rather mixed (see Ashby et al., 2010 for a detailed discussion). To examine changes in cortical and subcortical activity over time, we divided our experiment into four different sets (120 trials/set, 2 sets/phase), each consisting of a complete set of unique stimulus combinations, and conducted an additional GLM analysis. If practice effects are present, then we would expect to observe gradual BOLD signal decrease in cortical regions, especially in the control network, and steady increase in subcortical regions. Hence, we focused our analyses on seven ROIs sensitive to the subjective SoE modulation: 1) The control network (dlPFC, SMA, and IPL) and the vmPFC defined from the LowP phase SoE modulation, and 2) the putamen, thalamus/midbrain, and cerebellum clusters identified from the HighP > LowP contrast (see Tables 4 and 5). Specifically, to investigate overall changes in trial-induced activation over time, we extracted and averaged the percent signal changes and the parameter estimates,  $\beta_{\text{Trial}}$ , in the seven ROIs.

Results from 2 (sets)  $\times$  2 (LowP/HighP phases) ANOVAs based on the average percent signal changes showed no significant effect of phase nor set in all seven ROIs ( $ps > 0.05$ ), suggesting that overall BOLD activation remained stable in these regions throughout the experiment (see Fig. S1 and Table S1 in Supplementary Material). The mean  $\beta_{\text{Trial}}$ , however, demonstrated significant effects of phase for cognitive control regions (dlPFC:  $F_{(1,24)} = 24.02, p < 0.001$ ; SMA:  $F_{(1,24)} = 15.66, p = 0.001$ ; IPL:  $F_{(1,24)} = 26.44, p < 0.001$ ) as well as subcortical regions (putamen:  $F_{(1,24)} = 4.59, p = 0.04$ ; thalamus/midbrain:  $F_{(1,24)} = 5.97, p = 0.02$ ) and the cerebellum ( $F_{(1,24)} = 23.23, p < 0.001$ ), all of which exhibited an overall increase in trial-evoked response during the HighP phase. No effect of set nor phase  $\times$  set interaction was found ( $ps > 0.05$ ). In other words, we did not observe the gradual changes in activity predicted by the practice effect hypothesis, but rather a stepwise increase when moving from the low-pressure to the high-pressure phase.

Finally, to account for within-phase strategy variability influencing our neural data, we repeated decision strategy model selection using four sets (2 sets/phase) (Fig. S2A). We observed no changes in the overall winning model (i.e., model with the highest exceedance probability) within each phase. There was, however, an increased tendency of switching to Model 11 in the second set of the LowP phase, possibly a sign of satisficing behavior induced by extended exposure to the task. In the first set of the HighP phase, participants adopted an even more constricted cue space, with exceedance probabilities spreading out to Model 11 ( $c_1, c_2, c_3$ ), Model 5 ( $c_1, c_2$ ), and Model 1 ( $c_1$ ), thereby reflecting substantial behavioral changes triggered by the onset of severe time pressure. These time pressure induced changes in choice strategy are of course in accordance with our “drop-the-worst” proposal.

To ensure that this observed strategy variability does not strongly influence our neural results, we further contrasted fMRI data of the first set of the LowP phase (highest reliability in using the optimal model) versus the first set of the HighP phase (highest probability of adopting sub-optimal satisficing strategy) (Fig. S2B-D, Table S2). Consistent with our previous report, under low time pressure, the vmPFC and cognitive control network were significantly modulated by subjective SoE, whereas under high time pressure, increased modulation of the subcortical regions was observed. Hence, although some variability in cue usage exists within each phase and participants, the overall picture in terms of neuroimaging results does not differ much when individual sets are being

considered as compared to collapsing across sets within each phase.

In sum, both behavioral and neural evidence speak quite strongly against the possibility that the neural correlates of the phase-dependent decision-making shifts we report here are simply reflecting practice effects. The significant between-phase differences, in the absence of gradual behavioral and BOLD signal changes, are more likely to reflect strategy changes triggered by the time pressure manipulation.

#### 4. Discussion

To characterize neural mechanisms underlying satisficing decision-making induced by time pressure, we tested participants on a multi-cue probabilistic classification task under conditions of low (1500 ms) and high (500 ms) pressure during fMRI. Specifically, we focused on investigating post-learning decision performance, after participants had formed an understanding of the predefined cue structure through trial-and-error feedback learning. Using subjective cue weights and SoE inferred from a variational Bayesian approach, we demonstrate that, under low time pressure, participants accurately ranked the cues and integrated all available information to achieve near-optimal performance. Under this condition, distributed fMRI patterns in the dorsal striatum, dlPFC, and PCC could be used to make linear predictions about the subjective cue weights. Additionally, the total amount of evidence, quantified by subjective SoE, was encoded in the vmPFC, PCC, putamen, and hippocampus, whereas decision uncertainty was represented in the fronto-parietal cognitive control network. Under high time pressure, by contrast, participants adopted a drop-the-worst satisficing strategy by discounting the least important cue from their decision process, which was accompanied by an overall deterioration of performance and cue information encoding in the brain. Despite this degradation of information processing, we found significantly greater subjective SoE modulation under high time pressure in the putamen, dopaminergic midbrain, thalamus, and cerebellum. These findings suggest that time pressure triggers a shift from near-optimal decision-making dependent on both subcortical and fronto-parietal regions to satisficing decision-making characterized by a greater involvement of the midbrain, striatum, thalamus, and cerebellum.

Learning to perform probabilistic classification is thought to mainly rely on an interplay between the striatum and the hippocampus (Knowlton et al., 1996; Packard and Knowlton, 2002; Squire and Zola, 1996). The striatum serves an essential role in acquiring probabilistic cue-outcome associations in the weather prediction task (Knowlton et al., 1996; Poldrack et al., 2001) as well as other choice tasks that involve learning from reinforcement (Daw and Doya, 2006; Delgado et al., 2000; O'Doherty et al., 2003; Schultz, 1998; Schultz et al., 1997). Stress, induced by a socially evaluated cold pressor test, has been shown to trigger increased engagement of striatum-dependent implicit learning and impair the use of the hippocampus-dependent declarative system during probabilistic classification learning (Schwabe and Wolf, 2012). This shift to striatum-mediated learning has also been found when participants performed the weather prediction task under cognitive load (Foerde et al., 2006). In studies of the speed-accuracy tradeoff, increased activation was found in the striatum during trials with speed emphasis compared to trials with accuracy emphasis (Forstmann et al., 2008; van Veen et al., 2008), suggesting that enhanced striatal activity may be critical in reducing inhibitory control and facilitating speeded responses (Bogacz et al., 2010). Here, we significantly expand these findings by directly demonstrating that increased time pressure decreases the involvement of frontal and parietal regions and shifts probabilistic multi-cue decision-making to the striatum, even after the completion of initial cue learning.

In addition to the striatum, the midbrain (SN/VTA), and thalamus demonstrated significantly enhanced encoding of subjective SoE under high time pressure. Dopaminergic neurons in the SN/VTA are associated with expected rewards (D'Ardenne et al., 2008; Schultz et al., 1997) and control of motor responses (e.g., Hikosaka, 1989; Chevalier and Deniau,

1990; Mink, 1996) in decision-making. The thalamus serves as a critical relay structure between cortical and subcortical regions, facilitating information integration among the SN/VTA and striatum as well as prefrontal areas such as the vmPFC and dlPFC (Haber and Knutson, 2009). The vmPFC has been widely implicated in subjective value encoding (Daw et al., 2006; Kable and Glimcher, 2007; Levy and Glimcher, 2012; Montague and Berns, 2002; Padoa-Schioppa and Assad, 2006; Plassmann et al., 2007) and has been shown to integrate value information during multi-attribute decision-making (Basten et al., 2010; Hare et al., 2011; Kahnt et al., 2011). Building on these findings, we here show that vmPFC encodes integrated cue values. Under high time pressure, this SoE encoding was accompanied by enhanced modulation of the midbrain and striatal-thalamic circuit, suggesting that these regions may particularly facilitate information integration and evaluation when a speeded response is required.

We also found a significant modulatory effect of decision uncertainty on a fronto-parietal network that is consistently recruited during top-down attentional control processes that assist goal-directed behavior under cognitively demanding conditions (Dosenbach et al., 2006; Duncan and Owen, 2000; Niendam et al., 2012; Wager et al., 2004). In a multi-cue decision environment where only a single dimension is relevant, this network is involved in selecting the relevant feature, effectively reducing the dimensionality of the problem (Niv et al., 2015). In the current study, the dlPFC encoded individual cue weights as well as combined SoE, indicating that this region may be directly involved in the cue integration process. This is consistent with prior reports demonstrating engagement of the dlPFC in evidence accumulation during perceptual decision-making (Gold and Shadlen, 2007; Heekeren et al., 2008), and encoding of ambiguity or difficulty in multi-attribute decision-making (Kahnt et al., 2011; Krebs et al., 2012). Our results further demonstrate involvement of the fronto-parietal control network in a *feature-invariant* evidence integration processes, possibly guiding attention to cues according to their weighted importance and tracking uncertainty in choices.

Interestingly, the cerebellum was also involved in both cue value encoding and subjective SoE modulation under high time pressure. The cerebellum is traditionally regarded as contributing to movement planning and execution (Itō, 1984), and its role in cognitive functions is not well understood. Due to this structure's extensive connections to the cerebral cortex, including prefrontal areas (Habas et al., 2009), it has been suggested that the cerebellum may contribute to higher-level cognition, such as learning from feedback, which can support fast and adaptive control of motor behavior (Buckner, 2013; Ito, 2008; Strick et al., 2009). Hence, in the current task, the cerebellum may carry decision-relevant signals to facilitate quick motor responses. Although it is difficult to determine the precise role of the cerebellum in satisficing in the current study, the apparent involvement of this structure in fast-paced probabilistic inference represents an interesting starting point for future studies.

Although the use of heuristics is ubiquitous in everyday life, most neuroimaging studies on decision-making have focused on rather simple scenarios, where all decision-relevant information is available and participants are assumed to use a uniform, optimal strategy. Hence, neural mechanisms underlying heuristic processes that are used to simplify complex decision problems are not well understood (Volz and Gigerenzer, 2012). Prior studies that did examine neural correlates of heuristic decisions have largely focused on memory-guided heuristics (Khader et al., 2015, 2011; Rosburg et al., 2011; Volz et al., 2010, 2006). Given this focus on cached decision strategies and extensive training of explicit task rules, this prior work did not necessarily address how people arrive at decisions in more complex and natural decision environments. To overcome this problem, we used a large set of non-deterministic cue combinations, encouraging participants to actively integrate available information on each trial. Our study, therefore, provides novel evidence concerning the neural substrates of satisficing decision-making in the context of active, speeded cue integration.

We show that participants discounted the least important cue in their

decision processes under high time pressure, consistent with our previous findings (Oh et al., 2016). Participants performed at chance when the least important cue was the only differentiating cue between the two compound stimuli (Fig. 2B), indicating that the use of the drop-the-worst heuristic is a strategic choice, rather than due to having insufficient time to evaluate evidence. Where in the brain might cue information be “dropped” when decisions are made under high time pressure? It is possible that the deterioration in cue processing occurs at the sensory level (i.e., Ho et al., 2012) or alternatively, that it takes place at a later stage of the decision-making process. Due to an insufficient number of trials where only a single cue differentiated the competing stimuli, our current paradigm could not provide an unambiguous answer to this question. Despite this limitation, it is clear from the present data that the dopaminergic midbrain, striatum, and cerebellum encode subjective SoE preferentially under time pressure, and thus are key structures for facilitating satisficing decision-making.

In conclusion, the current study shows that near-optimal performance in multi-cue probabilistic classification under low time pressure is supported by widely distributed regions including both subcortical (striatum and hippocampus) and cortical (frontal and parietal) areas. Under high time pressure, by contrast, participants adopted the drop-the-worst satisficing strategy, which is characterized by increased involvement of the dopaminergic midbrain, thalamus, striatum, and cerebellum in mediating fast and good-enough decision-making.

### Conflicts of interest

The authors declare no competing financial interest.

### Acknowledgements

We thank John-Dylan Haynes for helpful discussions concerning the fMRI data analysis. This work was funded by Office of Naval Research grant ONR N000141310561.

### Appendix A. Supplementary data

Supplementary data related to this article can be found at <https://doi.org/10.1016/j.neuroimage.2017.08.069>.

### References

- Akaishi, R., Kolling, N., Brown, J.W., Rushworth, M., 2016. Neural mechanisms of credit assignment in a multicue environment. *J. Neurosci.* 36, 1096–1112. <http://dx.doi.org/10.1523/JNEUROSCI.3159-15.2016>.
- Ashby, F.G., Turner, B.O., Horvitz, J.C., 2010. Cortical and basal ganglia contributions to habit learning and automaticity. *Trends Cogn. Sci.* 14, 208–215. <http://dx.doi.org/10.1016/j.tics.2010.02.001>.
- Basten, U., Biele, G., Heekeren, H.R., Fiebach, C.J., 2010. How the brain integrates costs and benefits during decision making. *Proc. Natl. Acad. Sci. U. S. A.* 107, 21767–21772. <http://dx.doi.org/10.1073/pnas.0908104107>.
- Bogacz, R., Wagenmakers, E.J., Forstmann, B.U., Nieuwenhuis, S., 2010. The neural basis of the speed-accuracy tradeoff. *Trends Neurosci.* 33, 10–16. <http://dx.doi.org/10.1016/j.tins.2009.09.002>.
- Buckner, R.L., 2013. The cerebellum and cognitive function: 25 years of insight from anatomy and neuroimaging. *Neuron* 80, 807–815. <http://dx.doi.org/10.1016/j.neuron.2013.10.044>.
- Chevalier, G., Deniau, J.M., 1990. Disinhibition as a basic process in the expression of striatal functions. *Trends Neurosci.* 13, 277–280.
- D'Ardenne, K., McClure, S.M., Nystrom Leigh, E., Cohen, J.D., 2008. BOLD responses reflecting dopaminergic signals in the human ventral tegmental area. *Science* (80) 319, 1264–1267. <http://dx.doi.org/10.1126/science.1229223>.
- Daw, N.D., Doya, K., 2006. The computational neurobiology of learning and reward. *Curr. Opin. Neurobiol.* 16, 199–204. <http://dx.doi.org/10.1016/j.conb.2006.03.006>.
- Daw, N.D., O'Doherty, J.P., Dayan, P., Seymour, B., Dolan, R.J., 2006. Cortical substrates for exploratory decisions in humans. *Nature* 441, 876–879. <http://dx.doi.org/10.1038/nature04766>.
- Delgado, M.R., Nystrom, L.E., Fissell, C., Noll, D.C., Fiez, J.A., 2000. Tracking the hemodynamic responses to reward and punishment in the striatum. *J. Neurophysiol.* 84, 3072–3077. [http://dx.doi.org/10.1016/0166-2236\(90\)90107-1](http://dx.doi.org/10.1016/0166-2236(90)90107-1).
- Dias-Ferreira, E., Sousa, J.C., Melo, I., Morgado, P., Mesquita, A.R., Cerqueira, J.J., Costa, R.M., Sousa, N., 2009. Chronic stress causes frontostriatal reorganization and affects decision-making. *Science* (80) 325, 621–625.
- Dosenbach, N.U.F., Visscher, K.M., Palmer, E.D., Miezin, F.M., Wenger, K.K., Kang, H.C., Burgund, E.D., Grimes, A.L., Schlaggar, B.L., Petersen, S.E., 2006. A core system for the implementation of task sets. *Neuron* 50, 799–812. <http://dx.doi.org/10.1016/j.neuron.2006.04.031>.
- Doyon, J., Bellec, P., Amsel, R., Penhune, V., Monchi, O., Carrier, J., Lehericy, S., Benali, H., 2009. Contributions of the basal ganglia and functionally related brain structures to motor learning. *Behav. Brain Res.* 199, 61–75. <http://dx.doi.org/10.1016/j.bbr.2008.11.012>.
- Drugowitsch, J., 2013. Variational Bayesian Inference for Linear and Logistic Regression, vol. 1, pp. 1–13. arXiv:1310.5438.
- Duncan, J., Owen, A.M., 2000. Common regions of the human frontal lobe recruited by diverse cognitive demands. *Trends Neurosci.* 23, 475–483. [http://dx.doi.org/10.1016/S0166-2236\(00\)01633-7](http://dx.doi.org/10.1016/S0166-2236(00)01633-7).
- Foerster, K., Knowlton, B.J., Poldrack, R.A., 2006. Modulation of competing memory systems by distraction. *Proc. Natl. Acad. Sci. U. S. A.* 103, 11778–11783. <http://dx.doi.org/10.1073/pnas.0602659103>.
- Forstmann, B.U., Dutilh, G., Brown, S., Neumann, J., von Cramon, D.Y., Ridderinkhof, K.R., Wagenmakers, E.-J., 2008. Striatum and pre-SMA facilitate decision-making under time pressure. *Proc. Natl. Acad. Sci. U. S. A.* 105, 17538–17542. <http://dx.doi.org/10.1073/pnas.0805903105>.
- Friston, K., Holmes, A., Worsley, K., Polin, J., Frith, C., Frackowiak, R., 1994. Statistical parametric maps in functional imaging: a general linear approach. *Hum. Brain Mapp.* 2 (2), 189–210.
- Gluck, M., Bower, G., 1988. From conditioning to category learning: an adaptive network model. *J. Exp. Psychol. Gen.* 117, 227–247.
- Gold, J.I., Shadlen, M.N., 2007. The neural basis of decision making. *Annu. Rev. Neurosci.* 30, 535–574. <http://dx.doi.org/10.1146/annurev.neuro.29.051605.110308>.
- Habas, C., Kamdar, N., Nguyen, D., Prater, K., Beckmann, C.F., Menon, V., Greicius, M.D., 2009. Distinct cerebellar contributions to intrinsic connectivity networks. *J. Neurosci.* 29, 8586–8594. <http://dx.doi.org/10.1523/JNEUROSCI.1868-09.2009>.
- Haber, S.N., Knutson, B., 2009. The reward circuit: linking primate anatomy and human imaging. *Neuropsychopharmacology* 35, 4–26. <http://dx.doi.org/10.1038/npp.2009.129>.
- Hare, T.A., Malmaud, J., Rangel, A., 2011. Focusing attention on the health aspects of foods changes value signals in vmPFC and improves dietary choice. *J. Neurosci.* 31, 11777–11087. <http://dx.doi.org/10.1523/JNEUROSCI.6383-10.2011>.
- Haynes, J.D., Sakai, K., Rees, G., Gilbert, S., Frith, C., Passingham, R.E., 2007. Reading hidden intentions in the human brain. *Curr. Biol.* 17, 323–328. <http://dx.doi.org/10.1016/j.cub.2006.11.072>.
- Heekeren, H.R., Marrett, S., Ungerleider, L.G., 2008. The neural systems that mediate human perceptual decision making. *Nat. Rev. Neurosci.* 9, 467–479. <http://dx.doi.org/10.1038/nrn2374>.
- Hikosaka, O., 1989. Role of basal ganglia in initiation of voluntary movements. In: *Dynamic Interactions in Neural Networks: Models and Data*. Springer, New York, pp. 153–167.
- Ho, T., Brown, S., van Maanen, L., Forstmann, B.U., Wagenmakers, E.-J., Serences, J.T., 2012. The optimality of sensory processing during the speed-accuracy tradeoff. *J. Neurosci.* 32, 7992–8003. <http://dx.doi.org/10.1523/jneurosci.0340-12.2012>.
- Ito, M., 2008. Control of mental activities by internal models in the cerebellum. *Nat. Rev. Neurosci.* 9, 304–313. <http://dx.doi.org/10.1038/nrn2332>.
- Itô, M., 1984. *The Cerebellum and Neural Control*. Raven Pr.
- Kable, J.W., Glimcher, P.W., 2007. The neural correlates of subjective value during intertemporal choice. *Nat. Neurosci.* 10, 1625–1633. <http://dx.doi.org/10.1038/nn2007>.
- Kahnt, T., Heinze, J., Park, S.Q., Haynes, J.-D., 2011. Decoding different roles for vmPFC and dlPFC in multi-attribute decision making. *Neuroimage* 56, 709–715. <http://dx.doi.org/10.1016/j.neuroimage.2010.05.058>.
- Kelly, A.M.C., Garavan, H., 2005. Human functional neuroimaging of brain changes associated with practice. *Cerebr. Cortex* 15, 1089–1102. <http://dx.doi.org/10.1093/cercor/bhi005>.
- Khader, P.H., Pachur, T., Meier, S., Bien, S., Jost, K., Rösler, F., 2011. Memory-based decision-making with heuristics: evidence for a controlled activation of memory representations. *J. Cogn. Neurosci.* 23, 3540–3554. [http://dx.doi.org/10.1162/jocn\\_a.00059](http://dx.doi.org/10.1162/jocn_a.00059).
- Khader, P.H., Pachur, T., Weber, L.A., Jost, K., 2015. Neural signatures of controlled and automatic retrieval processes in memory-based decision-making. *J. Cogn. Neurosci.* 28, 69–83. <http://dx.doi.org/10.1162/jocn>.
- Knowlton, B., Mangels, J., Squire, L., 1996. A neostriatal habit learning system in humans. *Science* (80) 273, 1399–1402.
- Knowlton, B., Squire, L., Gluck, M., 1994. Probabilistic classification learning in amnesia. *Learn. Mem.* 1, 106–120. <http://dx.doi.org/10.1101/lm.1.2.106>.
- Krebs, R.M., Boehler, C.N., Roberts, K.C., Song, A.W., Woldorff, M.G., 2012. The involvement of the dopaminergic midbrain and cortico-striatal-thalamic circuits in the integration of reward prospect and attentional task demands. *Cerebr. Cortex* 22, 607–615. <http://dx.doi.org/10.1093/cercor/bhr134>.
- Kriegeskorte, N., Goebel, R., Bandettini, P., 2006. Information-based functional brain mapping. *Proc. Natl. Acad. Sci. U. S. A.* 103, 3863–3868. <http://dx.doi.org/10.1073/pnas.0600244103>.
- Lamberts, K., 2000. Information-accumulation theory of speeded categorization. *Psychol. Rev.* 107, 227–260. <http://dx.doi.org/10.1037/0033-295X.107.2.227>.
- Lehericy, S., Benali, H., Van de Moortele, P.-F., Pélégriani-Issac, M., Waechter, T., Ugurbil, K., Doyon, J., 2005. Distinct basal ganglia territories are engaged in early and advanced motor sequence learning. *Proc. Natl. Acad. Sci. U. S. A.* 102, 12566–12571. <http://dx.doi.org/10.1073/pnas.0502762102>.

- Levy, D.J., Glimcher, P.W., 2012. The root of all value: a neural common currency for choice. *Curr. Opin. Neurobiol.* 22, 1027–1038. <http://dx.doi.org/10.1016/j.conb.2012.06.001>.
- Maldjian, J.A., Laurienti, P.J., Burdette, J.H., 2004. Precentral gyrus discrepancy in electronic versions of the Talairach atlas. *Neuroimage* 21, 450–455. <http://dx.doi.org/10.1016/j.neuroimage.2003.09.032>.
- Maldjian, J.A., Laurienti, P.J., Kraft, R.A., Burdette, J.H., 2003. An automated method for neuroanatomic and cytoarchitectonic atlas-based interrogation of fMRI data sets. *Neuroimage* 19, 1233–1239. [http://dx.doi.org/10.1016/S1053-8119\(03\)00169-1](http://dx.doi.org/10.1016/S1053-8119(03)00169-1).
- Mink, J.W., 1996. The basal ganglia: focused selection and inhibition of competing motor programs. *Prog. Neurobiol.* 50, 381–425. [http://dx.doi.org/10.1016/S0301-0082\(96\)00042-1](http://dx.doi.org/10.1016/S0301-0082(96)00042-1).
- Montague, P.R., Berns, G.S., 2002. Neural economics and the biological substrates of valuation. *Neuron* 36, 265–284. [http://dx.doi.org/10.1016/S0896-6273\(02\)00974-1](http://dx.doi.org/10.1016/S0896-6273(02)00974-1).
- Murty, V.P., Shermohammed, M., Smith, D.V., Carter, R.M., Huettel, S.A., Adcock, R.A., 2014. Resting state networks distinguish human ventral tegmental area from substantia nigra. *Neuroimage* 100, 580–589. <http://dx.doi.org/10.1016/j.neuroimage.2014.06.047>.
- Nichols, T., Brett, M., Andersson, J., Wager, T., Poline, J.B., 2005. Valid conjunction inference with the minimum statistic. *Neuroimage* 25, 653–660. <http://dx.doi.org/10.1016/j.neuroimage.2004.12.005>.
- Niendam, T.A., Laird, A.R., Ray, K.L., Dean, Y.M., Glahn, D.C., Carter, C.S., 2012. Meta-analytic evidence for a superordinate cognitive control network subserving diverse executive functions. *Cogn. Affect Behav. Neurosci.* 12, 241–268. <http://dx.doi.org/10.3758/s13415-011-0083-5>.
- Niv, Y., Daniel, R., Geana, A., Gershman, S.J., Leong, Y.C., Radulescu, A., Wilson, R.C., 2015. Reinforcement learning in multidimensional environments relies on attention mechanisms. *J. Neurosci.* 35, 8145–8157. <http://dx.doi.org/10.1523/JNEUROSCI.2978-14.2015>.
- O'Doherty, J.P., Dayan, P., Friston, K., Critchley, H., Dolan, R.J., 2003. Temporal difference models and reward-related learning in the human brain. *Neuron* 28, 329–337. [http://dx.doi.org/10.1016/S0896-6273\(03\)00169-7](http://dx.doi.org/10.1016/S0896-6273(03)00169-7).
- O'Doherty, J.P., Kringelbach, M.L., Rolls, E.T., Hornak, J., Andrews, C., 2001. Abstract reward and punishment representations in the human orbitofrontal cortex. *Nat. Neurosci.* 4, 95–102. <http://dx.doi.org/10.1038/82959>.
- Oh, H., Beck, J.M., Zhu, P., Sommer, M.A., Ferrari, S., Egner, T., 2016. Satisficing in split-second decision making is characterized by strategic cue discounting. *J. Exp. Psychol. Learn. Mem. Cogn.* 42, 1937–1956. <http://dx.doi.org/10.1017/CBO9781107415324.004>.
- Packard, M.G., Knowlton, B.J., 2002. Learning and memory functions of the basal ganglia. *Annu. Rev. Neurosci.* 25, 563–593. <http://dx.doi.org/10.1146/annurev.immunol.22.012703.104702>.
- Padoa-Schioppa, C., Assad, J.A., 2006. Neurons in the orbitofrontal cortex encode economic value. *Nature* 441, 223–226. <http://dx.doi.org/10.1038/nature04676>.
- Payne, J., Bettman, J., Johnson, E., 1988. Adaptive strategy selection in decision making. *J. Exp. Psychol. Learn. Mem. Cogn.* 14, 534–552. <http://dx.doi.org/10.1037/0278-7393.14.3.534>.
- Plassmann, H., O'Doherty, J., Rangel, A., 2007. Orbitofrontal cortex encodes willingness to pay in everyday economic transactions. *J. Neurosci.* 27, 9984–9988. <http://dx.doi.org/10.1523/JNEUROSCI.2131-07.2007>.
- Poldrack, R., Clark, J., Paré-Blagoev, E., Shohamy, D., Creso Moyano, J., Myers, C., Gluck, M., 2001. Interactive memory systems in the human brain. *Nature* 414, 546–550. <http://dx.doi.org/10.1038/35107080>.
- Ratcliff, R., 1978. A theory of memory retrieval. *Psychol. Rev.* 85, 59–108. <http://dx.doi.org/10.1037/0033-295X.85.2.59>.
- Rieskamp, J., Hoffrage, U., 2008. Inferences under time pressure: how opportunity costs affect strategy selection. *Acta Psychol. Amst.* 127, 258–276. <http://dx.doi.org/10.1016/j.actpsy.2007.05.004>.
- Rigoux, L., Stephan, K.E., Friston, K.J., Daunizeau, J., 2014. Bayesian model selection for group studies - revisited. *Neuroimage* 84, 971–985. <http://dx.doi.org/10.1016/j.neuroimage.2013.08.065>.
- Rosburg, T., Mecklinger, A., Frings, C., 2011. When the brain decides: a familiarity-based approach to the recognition heuristic as evidenced by event-related brain potentials. *Psychol. Sci.* 22, 1527–1534. <http://dx.doi.org/10.1177/0956797611417454>.
- Schneider, W., Shiffrin, R.M., 1977. Controlled and automatic human information processing: I. Detection, search, and attention. *Psychol. Rev.* 84, 1–66. <http://dx.doi.org/10.1037/0033-295X.84.1.1>.
- Schultz, W., 1998. Predictive reward signal of dopamine neurons. *J. Neurophysiol.* 80, 1–27. <http://dx.doi.org/10.1007/s00429-010-0262-0>.
- Schultz, W., Dayan, P., Montague, P.R., 1997. A neural substrate of prediction and reward. *Science* (80) 275, 1593–1599. <http://dx.doi.org/10.1126/science.275.5306.1593>.
- Schwabe, L., Wolf, O.T., 2012. Stress modulates the engagement of multiple memory systems in classification learning. *J. Neurosci.* 32, 11042–11049. <http://dx.doi.org/10.1523/JNEUROSCI.1484-12.2012>.
- Schwabe, L., Wolf, O.T., 2009. Stress prompts habit behavior in humans. *J. Neurosci.* 29, 7191–7198. <http://dx.doi.org/10.1523/JNEUROSCI.0979-09.2009>.
- Shohamy, D., Myers, C., Grossman, S., Sage, J., Gluck, M., Poldrack, R., 2004. Corticostriatal contributions to feedback-based learning: converging data from neuroimaging and neuropsychology. *Brain* 127, 851–859. <http://dx.doi.org/10.1093/brain/awh100>.
- Simon, H., 1956. Rational choice and the structure of the environment. *Psychol. Rev.* 63, 129–138.
- Simon, H., 1955. A behavioral model of rational choice. *Q. J. Econ.* 69, 99–118.
- Squire, L.R., Zola, S.M., 1996. Structure and function of declarative and nondeclarative memory systems. *Proc. Natl. Acad. Sci. U. S. A.* 93, 13515–13522. <http://dx.doi.org/10.1073/pnas.93.24.13515>.
- Stephan, K.E., Penny, W.D., Daunizeau, J., Moran, R.J., Friston, K.J., 2009. Bayesian model selection for group studies. *Neuroimage* 46, 1004–1017. <http://dx.doi.org/10.1016/j.neuroimage.2009.03.025>.
- Strick, P.L., Dum, R.P., Fiez, J.A., 2009. Cerebellum and nonmotor function. *Annu. Rev. Neurosci.* 32, 413–434. <http://dx.doi.org/10.1146/annurev.neuro.31.060407.125606>.
- Van Turennout, M., Bielałowicz, L., Martin, A., 2003. Modulation of neural activity during object naming: effects of time and practice. *Cerebr. Cortex* 13, 381–391. <http://dx.doi.org/10.1093/cercor/13.4.381>.
- van Veen, V., Krug, M.K., Carter, C.S., 2008. The neural and computational basis of controlled speed-accuracy tradeoff during task performance. *J. Cogn. Neurosci.* 20, 1952–1965. <http://dx.doi.org/10.1162/jocn.2008.20146>.
- Volz, K.G., Gigerenzer, G., 2012. Cognitive processes in decisions under risk are not the same as in decisions under uncertainty. *Front. Neurosci.* 6, 105. <http://dx.doi.org/10.3389/fnins.2012.00105>.
- Volz, K.G., Schooler, L.J., Schubotz, R.I., Raab, M., Gigerenzer, G., von Cramon, D.Y., 2006. Why you think milan is larger than modena: neural correlates of the recognition heuristic. *J. Cogn. Neurosci.* 18, 1924–1936. <http://dx.doi.org/10.1162/jocn.2006.18.11.1924>.
- Volz, K.G., Schooler, L.J., von Cramon, D.Y., 2010. It just felt right: the neural correlates of the fluency heuristic. *Conscious. Cogn.* 19, 829–837. <http://dx.doi.org/10.1016/j.concog.2010.05.014>.
- Vulkan, N., 2000. An economist's perspective on probability matching. *J. Econ. Surv.* 14, 101–118. <http://dx.doi.org/10.1111/1467-6419.00106>.
- Wager, T.D., Jonides, J., Reading, S., 2004. Neuroimaging studies of shifting attention: a meta-analysis. *Neuroimage* 22, 1679–1693. <http://dx.doi.org/10.1016/j.neuroimage.2004.03.052>.
- Wright, P., 1974. The harassed decision maker: time pressures, distractions, and the use of evidence. *J. Appl. Psychol.* 59, 555–561. <http://dx.doi.org/10.1037/h0037186>.
- Yang, T., Shadlen, M.N., 2007. Probabilistic reasoning by neurons. *Nature* 447, 1075–1080. <http://dx.doi.org/10.1038/nature05852>.